

Adhesion and cleaning of foods with complex structure: effect of oil content and fluoropolymer coating characteristics on the detachment of cake from baking surfaces

Ole M. Magens¹, Yingda Liu¹, Jurgen F.A. Hofmans², Joke A. Nelissen² and D. Ian Wilson^{1*}

¹Department of Chemical Engineering and Biotechnology, University of Cambridge, New Museums Site, Pembroke Street, Cambridge, CB2 3RA, UK

²Chemours Belgium, A. Spinostraat 6A, 2800 Mechelen, Belgium

© OMM, YL, JH, JN and DiW

*Corresponding author

Email: diw11@cam.ac.uk

Tel. +44(0) 1223 334 777

Fax. + 44(0) 1223 334 796

Adhesion and cleaning of foods with complex structure: effect of oil content and fluoropolymer coating characteristics on the detachment of cake from baking surfaces

Ole M. Magens¹, Yingda Liu¹, Jurgen F.A. Hofmans², Joke Ann Nelissen² and D. Ian Wilson^{1*}

¹ Department of Chemical Engineering and Biotechnology, University of Cambridge, New Museums Site, Pembroke Street, Cambridge, CB2 3RA, UK

² Chemours Belgium, A. Spinostraat 6A, 2800 Mechelen, Belgium

* Corresponding author. Email: diw11@cam.ac.uk; Tel. +44(0) 1223 334 777; Fax. + 44(0) 1223 334 796

Abstract

The effect of surface coating on the detachment of a complex microstructured food material, was investigated using an improved version of the millimanipulation device described by Ali *et al.* (2015 *Food & Bioproducts Processing*, Vol. 93, 256-268). The test material was baked sponge cake batter, which contains approximately 27 vol% bubbles in a ‘continuous’ phase of emulsified oil in a flour/syrup suspension. Detachment in the dry state was studied for aluminium, 304 stainless steel and seven different fluoropolymer coatings. The surfaces differed in surface energy and roughness. The shear force required to detach baked cake, the work done, and the mass of residue remaining on the surface were measured. Virtually all samples detached by cohesive or mixed failure, where adhesion to the surface was stronger than or comparable with cohesive interactions within the cake. The shear force was almost independent of surface composition, energy and roughness, but strongly related to the oil content of the cake. The mass of residue was found to be linearly dependent on the calculated work of adhesion of oil to the surface in an aqueous environment. The quantitative findings are consistent with confocal microscopy images of uncooked batter contacting polar and non-polar surfaces which show very different oil spreading behaviour at the batter-substrate interface. The ability of oil to replace water from a surface is shown to be a key factor determining adhesion of these materials.

Keywords Adhesion, cake, cleaning, cohesion, fouling, surface energy

1 Introduction

The adhesive properties of soft solids on surfaces are critical for many industrial and household applications. Whilst adhesion is desired in many applications, such as coating operations, in others the adhesion of unwanted species and their accumulation to form fouling deposits or their retention as residual soiling layers is an ongoing problem. In the food sector the presence of such layers can reduce process efficiency and productivity. Their ability to harbour micro-organisms can compromise hygienic

operation, while cross-contamination (particularly in multi-product plant) can affect product quality or compromise batch integrity. Processes handling materials prone to adhere – which can be the product itself, as in heat exchanger fouling - are therefore subject to regular cleaning, monitoring and inspection.

Adhesion can often be managed by controlling the surface morphology and composition (Detry *et al.*, 2010). Coatings and surface modifications can mitigate the initiation and build-up of deposits and/or promote the release of soil under certain conditions, facilitating cleaning (Mérian and Goddard, 2012). In the cleaning map of Fryer and Asteriadou (2009), the promotion of soil release from the substrate provides an alternative to the use of chemical and/or thermal energy which would otherwise be needed to remove complex soils with strong cohesive interactions. Promoting soil release (termed adhesive failure by Fryer and Asteriadou) would in effect move the soil to a less complex region on their map.

Successful coatings can accrue long-term process cost savings (Gomes da Cruz *et al.*, 2014) as well as improving safety and hygiene.

Surface energy and work of adhesion

The scientific principles underpinning adhesion and cohesive interactions are well established. In an aqueous environment the forces between a substrate and an adhering layer are determined by contributions from electrostatic, Van der Waals, and solvation forces (Israelachvili, 2010). Since many soiling layers are many microns thick (they are visible to the naked eye) cohesive interactions also determine how the layer responds to an imposed force.

The surface topology and roughness play a role, by (i) determining the area available for interaction; (ii) controlling the interaction such as by the lotus leaf effect, where small, regular features modify the effective contact angle; and (iii) affecting the nature of the soiling layer, via the potential to promote nucleation (*e.g.* for crystallisation, see Junghahn, 1964, or condensation, see Zamuruyev *et al.*, 2014), and mechanical interlocking.

The surface tension of a liquid or the surface energy of a solid is classically treated as the sum of dispersion and polar forces, *i.e.* $\gamma = \gamma^d + \gamma^p$. Interfacial tensions obey the geometric mean ‘combination rules’ described by Fowkes (1963). For cases where both dispersive and polar interactions operate across the interface between medium 1 and 2 the interfacial tension is given by (Owens and Wendt, 1969)

$$\gamma_{12} = \gamma_1 + \gamma_2 - 2(\sqrt{\gamma_1^d \gamma_2^d} + \sqrt{\gamma_1^p \gamma_2^p}) \quad (1)$$

Here, γ_i is the surface tension between substance *i* and vacuum: the subscript for vacuum is omitted for convenience, as in many texts. Moreover, $\gamma_{i,\text{air}} \approx \gamma_i$. The thermodynamic work of adhesion in an

immersed system is estimated from the difference in total interfacial energy when adhering species 1 wets a substrate 2 in medium 3. As outlined by Clint and Wicks (2001), for an oil (1) to adhere to a solid substrate (2) when immersed in water (3), the work of adhesion, W_{123} is given by

$$W_{123} = \gamma_{23} + \gamma_{13} - \gamma_{12} \quad (2)$$

where γ_{23} , γ_{13} and γ_{12} are the interfacial tensions between substrate/water, oil/surrounding medium and oil/substrate, respectively. By combining Equations (1) and (2) it can be shown that

$$W_{123} = 2 \left(\gamma_3 + \sqrt{\gamma_1^d \gamma_2^d} + \sqrt{\gamma_1^p \gamma_2^p} - \sqrt{\gamma_2^d \gamma_3^d} - \sqrt{\gamma_2^p \gamma_3^p} - \sqrt{\gamma_1^d \gamma_3^d} - \sqrt{\gamma_1^p \gamma_3^p} \right) \quad (3)$$

Considering the relatively weak intermolecular interactions within and with a gas, for oil to attach to the same substrate when surrounded by air, W_{123} collapses to

$$W_{12} = 2 \left(\sqrt{\gamma_1^d \gamma_2^d} + \sqrt{\gamma_1^p \gamma_2^p} \right) \quad (4)$$

The oil will exhibit a contact angle, β , which is related to the interfacial energies by the Young-Laplace equation. Equation (2) then gives

$$W_{123} = \gamma_{13}(1 + \cos \beta) \quad (5)$$

The above relationships can be applied readily when the surface is uniform and there is one adhering species.

Food materials pose particular challenges when designing and predicting the performance of ‘non-stick’ coatings as a result of their multicomponent nature and heterogeneous microstructure. An aqueous solution may contain species which adsorb preferentially to different surfaces. Many foods feature emulsions with two liquid phases differing considerably in terms of hydrophobicity. This multiphase nature extends further with baked goods such as cake which may contain bubbles as well as solid components. This aspect, of variable microstructure and composition within a food material, is often neglected when considering adhesion to process surfaces. *A priori* prediction of adhesion of food materials is often, therefore, very approximate. Adhesion and removal behaviour of food and related structure products therefore have to be studied *in situ*, on the surface where they experience processing, under conditions which reflect those encountered during processing.

Measurement methods and experimental studies

Experimental techniques have been developed to study the adhesion or removal behaviour of complex soils on process surfaces. These can be categorised as applying a controlled or measured strain, or controlled stress, to the soil layer (Ali *et al.*, 2015). Hydrodynamic approaches employ controlled (or estimated) shear stress conditions and monitor the response. Examples include the parallel plate flow

cell and fluid dynamic gauging. These approaches provide useful information for design and operation when fluid flow is used to remove soils, *e.g.* in cleaning-in-place operations.

Controlled strain devices have been developed for studies at different length scales. Plynometers, which reproduce the rubbing action and frictional force imposed by hand cleaning, are used at the product length scale (Zorita *et al.*, 2010). Nano/microscale measurements are now possible: Mayer *et al.* (2012) measured the force required to dislodge individual CaCO₃ crystals with a bending-beam arrangement mounted in a scanning electron microscope chamber.

Capturing the contributions from different components of a composite, microstructured soil requires investigation at intermediate length scales. Zhang and co-workers (*e.g.* Akhtar *et al.*, (2010)) modified the micromanipulation technique originally developed to study deformation of cells (Zhang *et al.*, 1991) to investigate the adhesive and cohesive behaviour of fouling layers. In micromanipulation a stainless steel probe is dragged through the deposit at a set height relative to the substrate at a defined speed. This allows the forces to be measured and their variation with height to be quantified. Ali *et al.* (2015) developed a variant of this method which they called ‘millimanipulation’ to study viscoplastic layers at larger length scales. Ashokkumar and Adler-Nissen (2011) reported a similar scraping device to investigate the adhesion of foodstuffs (pancake, turkey meat, carrots and sweet potato) fried on different surfaces.

In the current work, three failure modes were observed which we label as adhesive, mixed, or cohesive (see *Figure 1*). The influence of adhesion and cohesion on removal behaviour were discussed by Hoseneey and Smewing (1999): sticky substances are associated with high adhesive forces and low cohesive forces. Adhesive failure occurs if the adhesive forces at the interface are weaker than the cohesive forces within the deposited material: the cake separates cleanly from the substrate, leaving little or no residual material. Conversely, in cohesive failure, breakage occurs at a shear plane within the cake, leaving a residual layer across the circular area of contact. Mixed failure arises when both occur, which is associated with the substrate surface and/or test material being heterogeneous. Non-stick coatings should promote adhesive failure, for ease of cleaning or for removal by forces exerted during processing.

Ashokkumar and co-workers (2011; 2010) evaluated the cleanability of different surfaces soiled by frying carrot, sweet potato, turkey meat and pancake at temperatures between 160 and 240°C with and without applying oil prior to frying. Their cleaning procedure involved water rinsing, soaking in cleaning solutions and scrubbing with different sponges. They reported significant effects of surface roughness on removal forces and amount of residue, which they related to bubble nucleation behaviour.

157 Smoother surfaces gave poorer removal performance. The pancakes studied in their frying experiments
158 featured porous structures generated by high heat fluxes which promote boiling and rapid moisture loss
159 on the heated surface.

160
161 Cake is an aerated food product and is likewise generated by baking a three-phase material, the batter.
162 The heat fluxes in baking are generally smaller and more uniform than in frying. During baking the air
163 bubbles present are expanded by the change in temperature, evaporation and release of carbon dioxide
164 from the degradation of baking soda. The ‘continuous phase’ is a multiphase dispersion, comprising an
165 emulsion of oil droplets in a suspension of flour particles in a sucrose solution. During baking, the starch
166 in the flour gelatinises and sets at higher temperatures to capture the structure (see Chesterton *et al.*,
167 2013). Whilst the characteristic sizes of surface active molecules and proteins are of order nanometres,
168 flour particles, oil droplets and air bubbles have diameters of tens to several hundred micrometres. The
169 material is therefore heterogeneous at different length scales and was chosen as a representative material
170 to test the performance of non-stick coatings for the food industry.

171
172 Coated baking trays are often used to minimise adhesion on baking lines. A new version of the
173 millimanipulation device reported by Ali *et al.* (2015) is employed here which allows a wider range of
174 forces to be studied. The removal characteristics of sponge cake prepared from a standard commercial
175 cake mix were studied for seven different fluoropolymer (FP) coated stainless steel plates, as well as
176 uncoated stainless steel and aluminium surfaces. The influence of surface topography as well as work
177 of adhesion, evaluated using Equation (3), were investigated. The effects of cake formulation and
178 baking time and were also studied and the findings are compared with the results reported for frying by
179 Ashokkumar and co-workers (2010; 2011; 2012).

180 **2 Materials and methods**

181 **2.1 Surfaces tested**

182 Table 1 is a summary of the surfaces investigated. The majority of substrate plates were 304 stainless
183 steel with dimensions either (i) square, 5×5 cm, thickness 2 mm (EN 1.4301 304, EN 10088-2 2R) or
184 (ii) circular, 5 cm diameter, 1 mm thick (EN 1.4301 304, EN 10088-2 2B). Chemours supplied five
185 different coated square and two coated circular substrates. Uncoated circular stainless steel and square
186 aluminium alloy substrates were included as references, representing metals commonly used in bakery
187 equipment. Surfaces were cleaned in dishwashing solution followed by rinsing with copious amounts
188 of tap water.

190 **2.1.1 Surface energies**

191 The dispersive and polar surface energy components of the test surfaces were determined according to
192 the Owens and Wendt (1969) model with water, formamide, ethylene glycol and dodecane. Twelve

contact angle measurements were taken for each liquid on each coating and the results are summarised in Table 2. PTFE-1 (used), SS and AL were strongly hydrophilic with surface energies more than twice the others. As expected, alongside with the other fully fluorinated coatings, the liquid based PTFE coating (PTFE-2) had a low total surface energy. Its dispersive and polar surface energy components are close to the values of $\gamma^d = 17 \text{ mJ/m}^2$ and $\gamma^p = 0.6 \text{ mJ/m}^2$ reported for PTFE by Clint and Wicks (2001). The non-zero polar component may arise from end-groups in the polymerisation reaction. The contact angle data were also analysed in terms of the van Oss *et al.* (1988) theory, which characterises the surface energy in terms of electron donor and acceptor sites. This indicated that electron donor components were dominant for all the surfaces tested (data not presented) and hence this theory was not used in the calculations as the system studied features no strong Lewis acid-acid or base-base repulsions.

After baking, indelible marks were evident on the PTFE-1 plates (see Supplementary Material 1), which remained after repeated cleaning in detergent solution. Contact angle measurements on the stained areas revealed that polar interactions had increased two-fold, while dispersive interactions decreased. This change is consistent with degradation of the epoxy resin during baking: this material is known to degrade at 180 °C.

2.1.2 Topology and roughness

The surface topology was scanned at five positions on each surface with a Zygo NewView 200 interferometer. The surface profile data were filtered with a 5×5 median filter and missing data were interpolated with a triangulation-based linear approach. Typical topology plots for each surface are shown in Figure 2. Both metal surfaces feature striations associated with machining and polishing. The arithmetic mean and root mean square roughness was calculated according to ISO 25178 are summarised in Table 1. Standard deviations were calculated on the basis of analysing the five profiles separately.

2.2 Cake material

A commercial cake mix (Betty Crocker™ Classic Vanilla Cake Mix) was used to generate cake test layers. Spray dried hen egg (internationalegg.co.uk) was used rather than fresh eggs to improve reproducibility. It was reconstituted with deionised water using a 12:37 mass ratio of egg powder to water. The typical ingredients of the cake mix and the spray dried egg as sold are given in Table 3. The total lipid content was varied between 6.11 wt% and 20.20 wt% by adding vegetable oil (100% rapeseed oil, Sainsbury's supermarket) while maintaining the masses of all other ingredients constant (see Table 4). The total constituent fractions of the cake batters were calculated by assuming that the fibre and salt fractions in the spray dried egg and the vegetable oil were negligible, as well as there being no water in the cake mix, egg powder and vegetable oil. The ingredients were combined in a large bowl with a

spatula, then whisked using a planetary mixer (Kenwood™ Chef KMC010) for 3 minutes at Setting 1 (67 rpm) until a smooth consistency was achieved. The air volume fraction of the batter, ϕ_{air} , calculated with Equation (6), was around 27 vol%.

$$\phi_{air} = 1 - \frac{\rho}{\rho_s} \quad (6)$$

Here ρ_s is the density of the deaerated suspension, obtained by centrifuging 50 mL samples at 1200 g for 15 min.

2.3 Confocal laser scanning microscopy

To visualise how the lipids in the batter interact with test surfaces, an oil soluble dye (9 wt% loading: oil Red O, Sigma Aldrich, dye content $\geq 75\%$) was mixed with rapeseed oil and filtered with a 0.45 μm pore size syringe filter (Sartorius Stedim Minisart®) before adding it to the batter mix. The dyed batter was then applied using a 20 ml BD™ syringe to (polar) borosilicate and (non-polar) polyvinyl chloride acetate (PVCA) cover slips. Confocal laser scanning microscopy was conducted on a Leica TCS SP5 microscope with an argon laser exciting the fluorophore at 514 nm, a 40 \times oil immersion lens (HCX PL APO 40 \times 1.25-0.75 oil) and the pinhole set at 60.6 μm .

2.4 Millimanipulation Device

The millimanipulation tool shown in Figure 3 offered superior and more flexible performance than the device reported by Ali *et al.* (2015). The sample is moved (the probe (1) is effectively static) and the force is measured by the transducer (2; 0 – 10 N or 0 – 20 N HBM S2M). The force measured by the transducer is amplified by a ratio set by the position of the transducer on the tower (3). The axis (4) can move at a steady speed, up to 20 mm/s, or move then rest with a full step resolution of 5 μm . These tests featured a sharp bottom edge on the probe, reducing the resistance from any material underneath the probe. The sample may be tested immersed in a temperature controlled bath (5), in ambient air on a plain sample holder (6).

Figure 4 (a) illustrates the millimanipulation action. A vertical blade is brought into contact with the layer (here, a small cake) and moved through the layer at a set speed, v . The voids in the structure render it compressible and the deformation induced by the blade motion (a combination of compliance and yield) detaches the cake in a complex fashion, often lifting it off at varying positions. This was overcome by baking cake samples in the holding ring device shown in Figure 4 (b and c). The test cake here is small compared to many baked products, starting as a short cylinder of batter with diameter, D , of 50 mm and height 10 mm. The wall of the holder is constructed from polytetrafluoroethylene (PTFE) and a grid of 316 stainless steel 1 mm diameter rods in the lower section ensures that the strain is transmitted evenly through the base layer of the cake. The cake then detaches across the substrate/cake interface

when the ring is moved laterally by the millimanipulation blade. As shown in Figure 4 (b), a pin on the blade ensures that the shear force is applied at the base of the ring. The contribution from the area under the PTFE ring to the force measured, F , is negligible. The process is videoed with a digital microscope and the amount and distribution of any residual layer remaining on the substrate recorded by imaging and weighing.

For experimental preparation the substrate plate and its test ring were each weighed before the latter was clamped onto the plate using three 51 mm fold-back clips. The compression provided by the clips prevented the ingress of batter beneath the ring which could result in an annulus of sticky material. 11.00 \pm 0.05 g of cake batter was filled into the chamber thus formed using a 20 ml BDTM syringe. Care was taken to fill the gaps between the rods so that the cake batter covered the coated plate completely. The ‘mini-cakes’ were baked in a pre-heated Carbolite[®] oven at 180°C for 8 minutes, then left to cool for 30 minutes in a temperature-controlled room at 22 \pm 1 °C. The clamps were then removed and the combined mass of the plate, test ring and cake was measured. The mass of the cooled cake weighed 9.37 g on average, representing a 15% mass loss on baking. Following millimanipulation testing the plate and any residual material was weighed and photographed.

Figure 5 (a) shows a typical force profile during a steady shear test. The signal is filtered with a finite impulse response band-stop filter to remove 50 Hz noise. After contact with the probe, setting $x = 0$, the force increases linearly with displacement up to about 4 N, after which the increase is non-linear, reaching a peak and falling sharply as the majority of the connections within the cake and/or between the cake and the surface rupture. This suggests that the material contains elastic elements with a distribution of limiting strains. Detailed interpretation of these results in terms of microstructural models was not attempted. Subsequently, the force decreases sharply and approaches a steady value associated with friction as the sheared material moves over the fracture plane. The low friction coefficient of PTFE and the light-weight ring (the average mass of the rings was 20.2 g) reduced the frictional contribution from the ring to less than 0.05 N during manipulation testing (measured without cake present).

The peak force F_{\max} is extracted from each force profile as indicated on the Figure and converted to the maximum shear stress, τ_{\max} , by dividing by the cake contact area. The breakage work per area (see Equation 7), W_b , is determined by calculating the work done (per unit area) from $x = 0$ to X , where X is the intercept on the x-axis of the projection of the tangent passing through the point of inflection, I, marked in Figure 5 (a):

$$W_b = \frac{1}{A} \int_0^x F dx \quad . \quad (7)$$

Figure 5 (b) shows the force profile obtained by a second mode of testing, labelled *relaxation testing*. The probe was moved 1 mm and then held in place for 20 s, labelled interval I, before being moved a further 1 mm, followed by 20 s delay (interval II), and then a further 1 mm (and interval III). The force decays with a quasi-exponential trend in interval I, indicating a visco-elastic response of the material. The peak force after interval I is similar to the initial value, but the decay response is very different: this feature, and the small force peak after interval II, indicates that rupture at the shear plane is complete. Further consideration of such data and analysis are not presented here: this mode of operation affords new insights into the material behaviour.

3 Results and Discussion

3.1 Removal behaviour

The majority of tests, on all surfaces and for all oil contents, featured cohesive or mixed failure (see Figure 1), leaving measurable amounts of residual material on the coated surface. This indicated that the strength of the adhesive interactions of the cake material with the surfaces was comparable or stronger than the cohesive interactions within the cake. The peak shear stress, τ_{\max} , and breakage work, W_b , should then both be influenced strongly by the forces required to disrupt the cake structure, and be less sensitive to the presence of a coating. The reverse would apply if the tests exhibited mostly adhesive failure. τ_{\max} and W_b showed a strong, positive correlation for all surfaces which confirms this hypothesis (see Supplementary Material 2). Cake with a high rapeseed oil content left lumps, a few mm in diameter, on the stainless steel surface. This indicates that the cohesive strength of the cake was weak compared to the material's adhesion to the steel. Peak shear stress is used as the indicator of forces in subsequent plots.

The effect of scraping speed, v , was investigated to see if this would promote a transition in breakage mechanism. Tests conducted with scraping speeds in the range 0.1 to 8 mm/s for the reference formulation on two fluoropolymer coated surfaces exhibited a logarithmic increase in τ_{\max} with v and no systematic difference in failure mode (data not reported).

3.2 Effect of cake formulation

Figure 6 and Table 5 indicate that the addition of oil reduces the cohesive strength of the cake. Figure 6 (b) shows that, with the exception of uncoated stainless steel, the peak shear stress decreases with increasing oil content up to about 8 wt% and is effectively constant thereafter. The similarity in trend for the remaining coatings and aluminium indicate that the contribution from surface properties is small by comparison, which is consistent with the hypothesis that τ_{\max} is determined by the cohesive strength of the cake material.

The τ_{\max} values for the PTFE-2 coating are twice as large as the other fluoropolymer coatings and decrease steadily with increasing oil content, unlike the other fluoropolymer coatings. This was the roughest surface tested, with S_a and S_q values of 2.3 μm and 2.8 μm , respectively, and maximum peak to valley distances of about 14 μm . The latter distance is large enough to harbour smaller flour particles. The large τ_{\max} values are not, however, accompanied by high m_{res} values, indicating that the large difference in surface roughness has caused a difference in the mechanical properties of the surface layer.

A simple explanation for the difference in τ_{\max} behaviour for the two metals is not available. The measured surface energy components are similar. The uncoated stainless steel is significantly smoother than the aluminium (Table 1) but this cannot be readily linked to the presence of a maximum in the cohesive forces. The thermal diffusivity of the aluminium is approximately 20 \times that of the stainless steel so the aluminium surface would be expected to reach the oven temperature more quickly. Temperature-driven hardening at the surface would then be expected to be manifested by greater adhesive or cohesive strength on the aluminium plates. This is not evident, and the similarity of the aluminium results to most of the coated surfaces indicates that heat transfer through the metal plate is not a significant factor. The additional thermal resistance imparted by coating is therefore not important. Similarly, the thickness of the plate had little effect.

Figure 6 (a) shows that the lipid content has a relatively small effect on the amount of residue with the exception of the uncoated stainless steel. The m_{res} values for all PFA coatings and FEP-2 are effectively constant, while FEP-1 shows a minimum around 12 wt% oil. Coating PTFE-1 gives m_{res} values similar to aluminium, both exhibiting a decrease in m_{res} with increasing cake oil content. The uncoated stainless steel results are again anomalous, giving values similar to the aluminium until 14 wt% and then a wide range of values at the highest oil loading. The anomalous datum of steel (20 wt% lipids), marked L, gave high m_{res} and low τ_{\max} values compared to the other steel tests (see also Table 5). This suggests a lower cohesive strength than adhesive strength, and is thought to arise from the oil preferring not to wet the surface but remaining in the bulk material.

The effect of surface energy on oil behaviour in the batter is demonstrated by the series of confocal microscopy images in

Figure 7, obtained with the 8 wt% oil content formulation on transparent surfaces. No baking was done. In (a), the microscope cover slip is made of strongly polar borosilicate glass whereas in (b) it is made from non-polar PVCA. Some oil droplets are evident suspended in the bulk of the dough whereas others are adhering to the substrates. The oil does not wet the polar borosilicate glass readily, instead forming discrete droplets with sizes up to 20 μm . The contact angle measured from the image is around 130°. The work of adhesion is low, estimated as 5.2 mJ/m² for an ideal system of rapeseed oil on borosilicate

glass when immersed in water. The contact angle calculated from Equation (5) was 154.2° (see Table 2 for calculated oil-surface-water contact angles), which is comparable with the observed value. The difference is attributed to surface active components and the batter's resistance to deformation.

In contrast, the work of adhesion of the oil on PVCA in water was calculated to be 91.5 mJ/m^2 . The affinity for the oil to stay at the non-polar polymer is demonstrated by Figure 7 (b), where the oil wets the PVCA surface readily and spreads across the surface. The contact angle is around 25° , which compares favourably with the value of 41.5° calculated for oil on PVCA in water. Quantitative analysis of the fluorescence intensity data (see Supplementary Material 3) showed the oil content to be greatest at the interface, whereas on the borosilicate glass the maximum oil content was located approximately $5 \mu\text{m}$ from the interface, which is consistent with the oleophobicity of the surface in an aqueous environment.

3.3 Effect of surface roughness

Surface roughness and surface energy have been reported to influence the performance of surface coatings. The influence of individual factors on m_{res} and low τ_{max} were quantified, for each oil content, and the Pearson correlation coefficients of the samples are presented in Table 6. Multi-variate techniques were not attempted as the results are unlikely to offer deterministic insight. The peak shear stress data do not show a systematic dependency on any of the parameters tested, with the largest coefficient being 0.69. This is consistent with τ_{max} being determined by forces involved in cohesive failure, which is expected to be determined chiefly by batter formulation rather than surface characteristics. Plots for peak shear stress over roughness for four batter formulations are provided in Supplementary Material 4.

The correlation coefficients for m_{res} for all oil contents studied show a very weak, negative correlation with S_a and S_q , indicating that there is little direct influence of surface roughness on the amount of residual layer. Similar findings were reported for bacterial adhesion on stainless steels by Detry *et al.*, (2010). An estimate of roughness-related coverage can be obtained by assuming that the support ring slides across the top of the highest asperities. The residual mass can then be estimated from the peak-to-valley dimension. This will be an overestimate. Taking the largest peak-to-valley value, $14 \mu\text{m}$ with PTFE-2, and batter density of approximately 950 kg/m^3 , gives a coverage of 13 g/m^2 . This is smaller than all those measured, and indicates that m_{res} is not determined by filling the surface features. The values measured on most of the coated plates, or $40\text{-}70 \text{ g/m}^2$, correspond to a layer thickness of $40\text{-}70 \mu\text{m}$, which is similar to the sizes of the structural components in the cake, *i.e.* the oil droplets ($5\text{-}20 \mu\text{m}$) and flour particles.

3.3 Work of adhesion

Table 6 reports a strong positive correlation between the residual mass and all three components of surface energy, particularly for γ^p , for which correlation coefficients ranged from 0.87 to 0.97. This result is consistent with the postulation of m_{res} being linked to oil wetting behaviour outlined above. A stronger, negative, correlation is evident when the surface energy components are combined in the theoretical work of wetting, W_{123} . Figure 8 (a) illustrates that a high work of adhesion of the oil phase, and thus its tendency to wet the surface, deters cake retention.

An explanation for this behaviour is that the surface coating determines whether the oil spreads readily across the surface or is present as discrete ‘islands’, resulting in different fractions of surface area in direct contact with the aqueous matrix. The cluster of smaller m_{res} values in Figure 14 (a) belong to surfaces with $\gamma_{12} < \gamma_{23}$, giving from Equations (2) and (5) an oil contact angle in water less than 90° , indicating that oil will prefer to spread on the substrate. The baking time is too short for the oil to react to give a cohesive material (8 minutes at 180°C is not sufficient time to cause polymerisation of the oil: Ali *et al.* (2015) baked their lard layers for several hours), whereas the starch and proteins in the matrix undergo various transformations in this time. The oil thus tends to shear rather than rupture during testing, requiring a smaller shear force. Regions with high matrix contact will register higher peak force. It should be noted that the W_{123} values are calculated for simple oil-matrix-substrate interactions and do not account for the volume fraction of oil in the batter, which will determine the availability of oil to coat the surface.

The results obtained for the 6.11 wt% lipid formulation, with no additional rapeseed oil, are presented in Figure 8 (b). This shows a similar trend but there is more scatter. In this case the lipids are palm fat and lipids present in the egg powder, a fraction of which are solid at room temperature. They are less mobile in terms of wetting and also provide stronger resistance to shear when tested at room temperature.

3.4 Discussion

Fluorocarbon-based coatings are often considered for ‘non-stick’ applications and many studies have demonstrated their effectiveness for food operations, including frying (Ashokkumar and Adler-Nissen, 2011), thermal processing of milk (Gomes da Cruz *et al.*, 2014) and handling caramel (Goode *et al.*, 2013). Goode *et al.* used atomic force microscopy to measure the adhesion forces between stainless steel or fluoro-coated glass (FCG) surfaces and (i) whey protein concentrate, (ii) sweetened condensed milk, and (iii) caramel, over the temperature range 30 to 90°C . The protein concentrate did not adhere strongly to FCG at temperatures up to 70°C but adhered strongly at 90°C , which is attributed to denaturation of the protein and a change in its surface characteristics. Caramel (containing 11 wt% fat) adhered strongly to FCG initially and this diminished with contact times longer than 1 s. The adhesion

of caramel at short contact times depended on temperature whereas it was independent of temperature at longer times, suggesting that the material involved in adhesion changed over the first second of contact. On the basis of the results presented above we postulate that this behaviour is related to the time for lipids to diffuse to and adsorb at the interface, replacing the polar aqueous phase.

It is interesting to compare these findings with the results for pancake frying reported by Ashokkumar *et al.* (2010). Their pancake formulations differed noticeably from the cake mixes studied here (egg white 13.3%, egg yolk 8%, milk 40%, 33.3% wheat flour, 5.3% sugar: water content 59.3%, all w.b.). The contact angle data from Ashokkumar *et al.* (2012) were used to estimate W_{123} for adhesion of the frying oil to the different surfaces, assuming an initially aqueous environment. In cases where no oil was added prior to frying the cleaning rating (a visual characterisation) was independent of W_{123} . When oil was added, the deposit was harder to clean from polar metallic surfaces (with lower W_{123} values), which is consistent with Figure 8. The simple work of adhesion model assumes a liquid water phase competing with the oil in wetting. During frying, bubble formation and water evaporation is likely to remove the water phase from the surface soon after contact, giving rise to the insensitivity to W_{123} .

The cake materials investigated here demonstrate that ‘non-stick’ behaviour is not universal and is determined by the surface and the soil properties. It would be a challenge to identify a surface which would resist attachment of this material as it contains three components with very different wetting characteristics: oil, a sugar/starch aqueous phase, and bubbles likely to have surface active proteins at the liquid/vapour interface. Moreover, the material is processed in such a way (semi-quiet baking) that allows adhering components to migrate to the surface.

Finally, it must be noted that cleaning with a liquid involves a new series of interactions and is likely to promote detachment of the residues, particularly if surfactants or shear forces are present. This highlights the difference between attachment and cleaning.

4 Conclusions

Millimanipulation was used to evaluate the performance of stainless steel plates coated with seven different fluorocarbon coatings, alongside stainless steel and aluminium surfaces as reference. The surface energies and topographies of the surfaces were measured and the former was used to calculate the ideal energy of wetting associated with oil attaching to the surface when immersed in water.

The removal tests were conducted in the dry state. There was little influence of scraping speed and surface roughness, but a strong sensitivity to cake oil content. This result, alongside the observation of residual material on all surfaces, confirmed that the cake was a sticky material wherein adhesion to the surface was stronger than cohesive interactions within the cake matrix. The removal forces were mostly

sensitive only to oil content, whereas the amount of residue was found to be directly related to the oil's work of adhesion to the surfaces assuming the cake matrix to resemble an aqueous environment.

The ability of oil to replace water from a surface seems to be a key mechanism for a 'non-stick' surface in baking applications involving water and oil containing doughs or oil pre-wetted moulds. In frying, where the foodstuff is placed on a hot surface, the situation is different. High temperatures evaporate water too quickly to allow the oil to be driven to the surface by hydrophobic repulsion.

Acknowledgements

A Jardine Postgraduate Scholarship for YL from the Jardine Foundation and a PhD studentship for OMM from Du Pont/Chemours and is gratefully acknowledged. The millimanipulation device was constructed to OMM's specifications by Gautrey Engineering, Cottenham, UK.

495 **Nomenclature (alphabetical order)**

496	A	cake contact area	m^2
497	D	diameter of test cake	m
498	F	force	N
499	m_{res}	residual mass per area	g/m^2
500	S_a	roughness according to ISO 25178, arithmetic mean	m
501	S_q	roughness according to ISO 25178, root mean square	m
502	W	adhesion/breakage work per area	J/m^2
503	v	millimanipulation velocity	m/s
504	x	scraping distance	m
505	X	upper integration limit in calculation of breakage work per area	m
506	Greek		
507	$\beta, \beta_{\text{ows}}$	contact angle, contact angle of oil in water on surface	$^\circ$
508	γ	surface energy, surface tension	mJ/m^2
509	ρ, ρ_s	density of the cake batter, centrifuged cake batter (suspension)	kg/m^3
510	τ, τ_{max}	shear stress, peak value	kPa
511	ϕ_{air}	air volume fraction	1
512	Subscripts		
513	1	adsorbing species	
514	2	surface	
515	3	surrounding medium	
516	b	breakage	
517	i	integer	
518	Superscripts		
519	d	dispersive	
520	p	polar	
521			

References

- Akhtar, N., Bowen, J., Asteriadou, K., Robbins, P.T., Zhang, Z., Fryer, P.J., 2010. Matching the nano- to the meso-scale: Measuring deposit-surface interactions with atomic force microscopy and micromanipulation. *Food Bioprod. Process.* 88, 341–348. doi:10.1016/j.fbp.2010.08.006
- Ali, A., De'Ath, D., Gibson, D., Parkin, J., Alam, Z., Ward, G., Wilson, D.I., 2015. Development of a “millimanipulation” device to study the removal of soft solid fouling layers from solid substrates and its application to cooked lard deposits. *Food Bioprod. Process.* 93, 256–268. doi:10.1016/j.fbp.2014.09.001
- Ashokkumar, S., Adler-Nissen, J., 2011. Evaluating non-stick properties of different surface materials for contact frying. *J. Food Eng.* 105, 537–544. doi:10.1016/j.jfoodeng.2011.03.018
- Ashokkumar, S., Adler-Nissen, J., Møller, P., 2012. Factors affecting the wettability of different surface materials with vegetable oil at high temperatures and its relation to cleanability. *Appl. Surf. Sci.* 263, 86–94.
- Ashokkumar, S., Thomsen, B.R., Raagaard, Hinke, J., Møller, P., Adler-Nissen, J., 2010. Cleanability Evaluation of Different Surfaces by Fouling from Contact Frying of Foods, in: *Fouling and Cleaning in Food Processing*. Cambridge University Press, pp. 24–33.
- Chesterton, A.K.S., De Abreu, D.A.P., Moggridge, G.D., Sadd, P.A., Wilson, D.I., 2013. Evolution of cake batter bubble structure and rheology during planetary mixing. *Food Bioprod. Process.* 91, 192–206. doi:10.1016/j.fbp.2012.09.005
- Clint, J.H., Wicks, A.C., 2001. Adhesion under water: Surface energy considerations. *Int. J. Adhes. Adhes.* 21, 267–273. doi:10.1016/S0143-7496(00)00029-4
- Detry, J.G., Sindic, M., Deroanne, C., 2010. Hygiene and cleanability: a focus on surfaces. *Crit. Rev. Food Sci. Nutr.* 50, 583–604. doi:10.1080/10408390802565913
- Esteban, B., Riba, J.-R., Baquero, G., Puig, R., Rius, A., 2012. Characterization of the surface tension of vegetable oils to be used as fuel in diesel engines. *Fuel* 102, 231–238. doi:10.1016/j.fuel.2012.07.042
- Fowkes, F.M., 1963. Additivity of Intermolecular Forces at Interfaces. I. Determination of the contribution to surface and interfacial tensions of dispersion forces in various liquids. *J. Phys. Chem.* 67, 2538–2541. doi:10.1021/j100806a008
- Fryer, P.J. and Asteriadou, K., 2009, A prototype cleaning map: a classification of industrial cleaning processes. *Trends Food Sci. Tech.* 20, 255–262. doi: 10.1016/j.tifs.2009.03.005.
- Gomes da Cruz, L., Ishiyama, E.M., Boxler, C., Augustin, W., Scholl, S., Wilson, D.I., 2014. Value pricing of surface coatings for mitigating heat exchanger fouling. *Food Bioprod. Process.* 93, 343–363. doi:10.1016/j.fbp.2014.05.003
- Goode, K.R.R., Bowen, J., Akhtar, N., Robbins, P.T.T., Fryer, P.J.J., 2013. The effect of temperature on adhesion forces between surfaces and model foods containing whey protein and sugar. *J. Food Eng.* 118, 371–379. doi:10.1016/j.jfoodeng.2013.03.016
- Hoseney, R.C., Smewing, J.O., 1999. Instrumental measurement of stickiness of doughs and other foods. *J. Texture Stud.* 30, 123–136. doi:10.1111/j.1745-4603.1999.tb00206.x

561 Israelachvili, J.N., 2010. Intermolecular and Surface Forces Third Edition. Intermol. Surf. Forces.
 562 doi:10.1016/B978-0-12-375182-9.10025-9

563 Junghahn, L., 1964. Methoden zum Herabsetzen oder Verhindern der Krustenbildung. Chemie Ing.
 564 Tech. - CIT 36, 60–67. doi:10.1002/cite.330360110

565 Mayer, M., Augustin, W., Scholl, S., 2012. Adhesion of single crystals on modified surfaces in
 566 crystallization fouling. J. Cryst. Growth 361, 152–158. doi:10.1016/j.jcrysgro.2012.09.032

567 Mérian, T., Goddard, J.M., 2012. Advances in nonfouling materials: Perspectives for the food
 568 industry. J. Agric. Food Chem. 60, 2943–2957. doi:10.1021/jf204741p

569 Owens, D.K., Wendt, R.C., 1969. Estimation of the surface free energy of polymers. J. Appl. Polym.
 570 Sci. 13, 1741–1747. doi:10.1592/phco.30.10.1004

571 van Oss, C.J., Chaudhury, M.K., Good, R.J., 1988. Interfacial Lifshitz-van der Waals and polar
 572 interactions in macroscopic systems. Chem. Rev. 88, 927–941. doi:10.1021/cr00088a006

573 van Oss, C.J., Giese, R.F.F., Li, Z., Murphy, K., Norris, J., Chaudhury, M.K.K., Good, R.J., 1992.
 574 Determination of contact angles and pore sizes of porous media by column and thin layer
 575 wicking. J. Adhes. Sci. Technol. 6, 413–428. doi:10.1163/156856192X00755

576 Zamuruyev, K.O., Bardaweel, H.K., Carron, C.J., Kenyon, N.J., Brand, O., Delplanque, J.P., Davis,
 577 C.E., 2014. Continuous droplet removal upon dropwise condensation of humid air on a
 578 hydrophobic micropatterned surface. Langmuir 30, 10133–10142. doi:10.1021/la5004462

579 Zhang, Z., Ferenczi, M.A., Lush, A.C., Thomas, C.R., 1991. A novel micromanipulation technique for
 580 measuring the bursting strength of single mammalian cells. Appl. Microbiol. Biotechnol. 36,
 581 208–210. doi:10.1007/BF00164421

582 Zorita, S., Niquet, C., Bonhoure, J., Robert, N., Tessier, F.J., 2010. Optimisation of a model food
 583 mixture using response surface methodology to evaluate the anti-adhesive properties of cooking
 584 materials. Int. J. Food Sci. Technol. 45, 2494–2501. doi:10.1111/j.1365-2621.2010.02459.x

585

Tables

Table 1: Summary of surfaces studied. S_a and S_q are, respectively, the arithmetic mean and root mean square roughness of the substrates. \pm indicates standard deviation.

Name	Symbol	Shape	Thickness (mm)	Surface	S_a (nm)	S_q (nm)
SS	▲	circular	1	stainless steel; EN 1.4301 304, EN 10088-2 2B	65 ± 9.6	90 ± 17
AL	△	square	1	aluminium alloy	351 ± 31	425 ± 37
PFA-1	■	circular	1	liquid based perfluoroalkoxy alkane (PFA)	1447 ± 205	1760 ± 240
PFA-2	■	square	2	powder based PFA	490 ± 47	610 ± 58
PFA-3	■	square	2	liquid based PFA	560 ± 67	700 ± 80
FEP-1	+	circular	1	liquid based fluorinated ethylene propylene (FEP)	380 ± 54	470 ± 65
FEP-2	×	square	2	liquid based FEP	380 ± 78	480 ± 92
PTFE-1	◇	square	2	epoxy resin with dispersed polytetra- fluoroethylene (PTFE) particles	740 ± 73	960 ± 110
PTFE-2	◆	square	2	liquid based PTFE	2290 ± 310	2810 ± 290

Table 2: Equilibrium contact angle, β , measured at 20 °C, and surface energy components calculated from the Owens and Wendt (1969) approach. \pm indicates 95 % confidence interval of the mean. Liquid parameters taken from (van Oss et al., 1992). β_{ows} is the contact angle for rapeseed oil ($\gamma^d = 33.8 \text{ mJ/m}^2$, $\gamma^p \approx 0 \text{ mJ/m}^2$; Esteban *et al.*, (2012) in water ($\gamma^d = 21.8 \text{ mJ/m}^2$, $\gamma^p = 51.0 \text{ mJ/m}^2$) on the surface calculated from Equation (5). Angles reported to one decimal place.

Liquid	ethylene				Surface energy (mJ/m ²)		β_{ows} (°)
	water	formamide	glycol	dodecane			
γ^d (mJ/m ²)	21.8	39.0	29.0	25.4			
γ^p (mJ/m ²)	51.0	19.0	19.0	0.0			
Surface	β (°)				γ^d	γ^p	
SS	64.3 \pm 1.9	61.5 \pm 2.0	51.8 \pm 2.9	4.0 \pm 0.9	18.4 \pm 5.2	21.0 \pm 5.9	98.8
AL	57.6 \pm 8.8	67.6 \pm 8.2	41.2 \pm 2.6	5.1 \pm 1.4	18.8 \pm 6.6	20.8 \pm 7.4	108.0
PFA-1	105.4 \pm 5.3	93.4 \pm 3.3	90.7 \pm 2.6	37.9 \pm 1.3	17.2 \pm 3.6	0.7 \pm 0.8	45.1
PFA-2	110.3 \pm 1.8	90.4 \pm 1.8	94.7 \pm 0.7	43.0 \pm 0.8	17.6 \pm 2.0	0.2 \pm 0.2	36.4
PFA-3	108.2 \pm 2.0	92.8 \pm 3.5	91.8 \pm 1.5	44.6 \pm 1.2	16.7 \pm 2.1	0.5 \pm 0.4	42.5
FEP-1	98.0 \pm 3.1	93.5 \pm 1.3	91.0 \pm 1.5	37.6 \pm 1.8	15.2 \pm 3.9	2.1 \pm 1.6	58.6
FEP-2	108.4 \pm 1.1	92.9 \pm 4.0	92.6 \pm 1.3	41.6 \pm 3.3	17.2 \pm 2.2	0.4 \pm 0.3	40.4
PTFE-1	81.1 \pm 3.5	70.1 \pm 2.8	65.7 \pm 2.9	19.3 \pm 7.3	20.8 \pm 3.2	7.2 \pm 2.0	77.9
PTFE-1 used	63.0 \pm 4.9	63.7 \pm 3.7	61.4 \pm 4.0	15.4 \pm 3.9	18.0 \pm 5.5	17.3 \pm 5.7	101.7
PTFE-2	106.9 \pm 4.7	96.3 \pm 2.0	96.3 \pm 3.0	38.1 \pm 2.6	16.2 \pm 3.8	0.5 \pm 0.7	42.6
borosilicate glass slip	11.3 \pm 1.13	9.7 \pm 0.69	8.4 \pm 0.16	0 \pm 0 ^a	20.5 \pm 4.7	45.6 \pm 7.5	154.2
PVCA slip	103.8 \pm 0.37	83.9 \pm 0.96	79.5 \pm 3.0	25.2 \pm 1.1	22.3 \pm 1.2	0.5 \pm 0.2	41.5

^a contact angle too small to identify, set to zero

599 Table 3: Ingredients and constituents of cake mix and spray dried egg, taken from packaging.
600

Betty Crocker™ Classic Vanilla Cake Mix		
Ingredients: sugar, wheat flour, palm fat, raising agents: monocalcium phosphate, sodium bicarbonate, modified corn starch, salt, Emulsifiers: propane- 1, 2-dial esters of fatty acids, mono-diglycerides of fatty acids, Flavouring, Stabiliser: Xanthan gum	Constituent	fraction (wt%)
	Fat	7.8 (of which 4.1 are saturates)
	Carbohydrates	79.3 (of which 47.1 are sugars)
	Fibre	1.4
	Protein	5.1
	Salt	1.6
Spray dried hen egg		
Ingredients: Pasteurised and spray dried hen eggs	Constituent	fraction (wt%)
	Fat	42
	Carbohydrates	5
	Protein	46

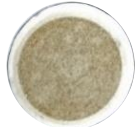


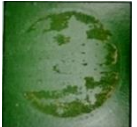



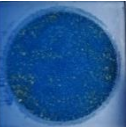











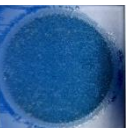



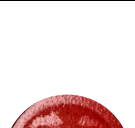







601

602 Table 4: Ingredients and total constituent fractions of the cake batter recipes used. **Bold** text indicates
603 preparation according to the recipe on the packaging.
604

Ingredient								
Cake mix (g)								135.00
Egg powder (g)								13.96
Deionised water (g)								118.94
Vegetable oil (g)	0.00	5.47	11.16	17.10	23.30	29.77	60.47	
Mass fraction in batter (all in wt%)								
lipids	6.11	8.00	9.87	11.75	13.63	15.51	20.20	
carbohydrates	40.22	39.42	38.61	37.81	37.00	36.20	32.81	
fibre	0.71	0.69	0.68	0.66	0.65	0.64	0.57	
protein	4.96	4.87	4.77	4.67	4.57	4.47	4.05	
salt	0.81	0.79	0.77	0.76	0.74	0.73	0.66	
water	44.40	43.51	42.62	41.73	40.85	39.96	36.22	

605

606 Table 5: Photos of typical residue left on the substrates after Millimanipulation for four different total lipid fractions. Anomalous case where lumps of cake
607 were left on SS plates at 20.2 wt% lipid is shown. Numbers are average residue masses in g/m² and ± indicate standard errors.

		Substrate (residue masses in g/m ²)								
		SS	AL	PFA-1	PFA-2	PFA-3	FEP-1	FEP-2	PTFE-1	PTFE-2
Lipid fraction (wt%)	6.11	 169 ±2.7	 149 ±5.9	 42 ±9.9	 37 ±14.0	 69 ±9.6	 80 ±16.9	 66 ±11.6	 133 ±2.7	 106 ±18.6
	8	 143 ±5.6	NA 145 ±7.5	 43 ±5.2	NA 37 ±8.2	NA 62 ±7.5	 72 ±2.5	NA 48 ±4.6	NA 130 ±7.0	NA 53 ±11.6
	13.63	 109 ±7.0	 119 ±10.3	 32 ±3.0	 34 ±11.9	 60 ±5.1	 54 ±9.5	 58 ±2.7	 121 ±6.8	 61 ±5.3
	20.2	 127 ±13.8	 115 ±8.3	 38 ±5.0	 32 ±4.6	 61 ±9.6	 80 ±3.2	 60 ±7.6	 96 ±7.6	 56 ±0
		 265 (lumps)								

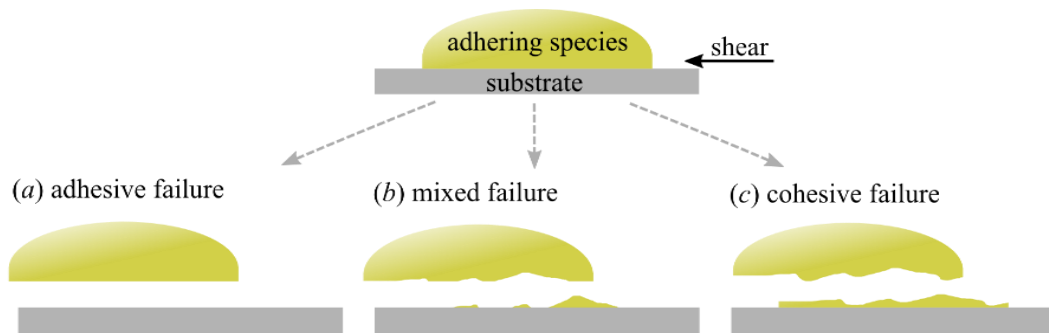
608

Table 6: Sample Pearson correlation coefficients between surface properties and residual mass and maximum shear stress for different total lipid contents. Coefficients in **bold** indicate highest correlation for a specific lipid content.

Lipid content	m_{res} (g/m ²)				τ_{max} (Pa)			
	6.11	8	13.63	20.2	6.11	8	13.63	20.2
γ	0.87	0.97	0.93	0.88	-0.038	0.0023	0.36	-0.072
γ^d	0.62	0.67	0.60	0.60	-0.33	-0.20	0.48	-0.38
γ^p	0.87	0.97	0.95	0.88	0.014	0.036	0.32	-0.017
W_{123}	-0.89	-0.99	-0.95	-0.91	0.0041	-0.072	-0.33	0.037
S_a	-0.22	-0.43	-0.33	-0.49	0.69	0.63	0.15	0.67
S_q	-0.21	-0.42	-0.33	-0.48	0.68	0.63	0.14	0.67
Substrate thickness	-0.31	-0.41	-0.17	-0.46	0.12	-0.044	-0.17	0.27

615 **Figures**

616



617

618

619 Figure 1: Schematic of the failure modes encountered in experiments.

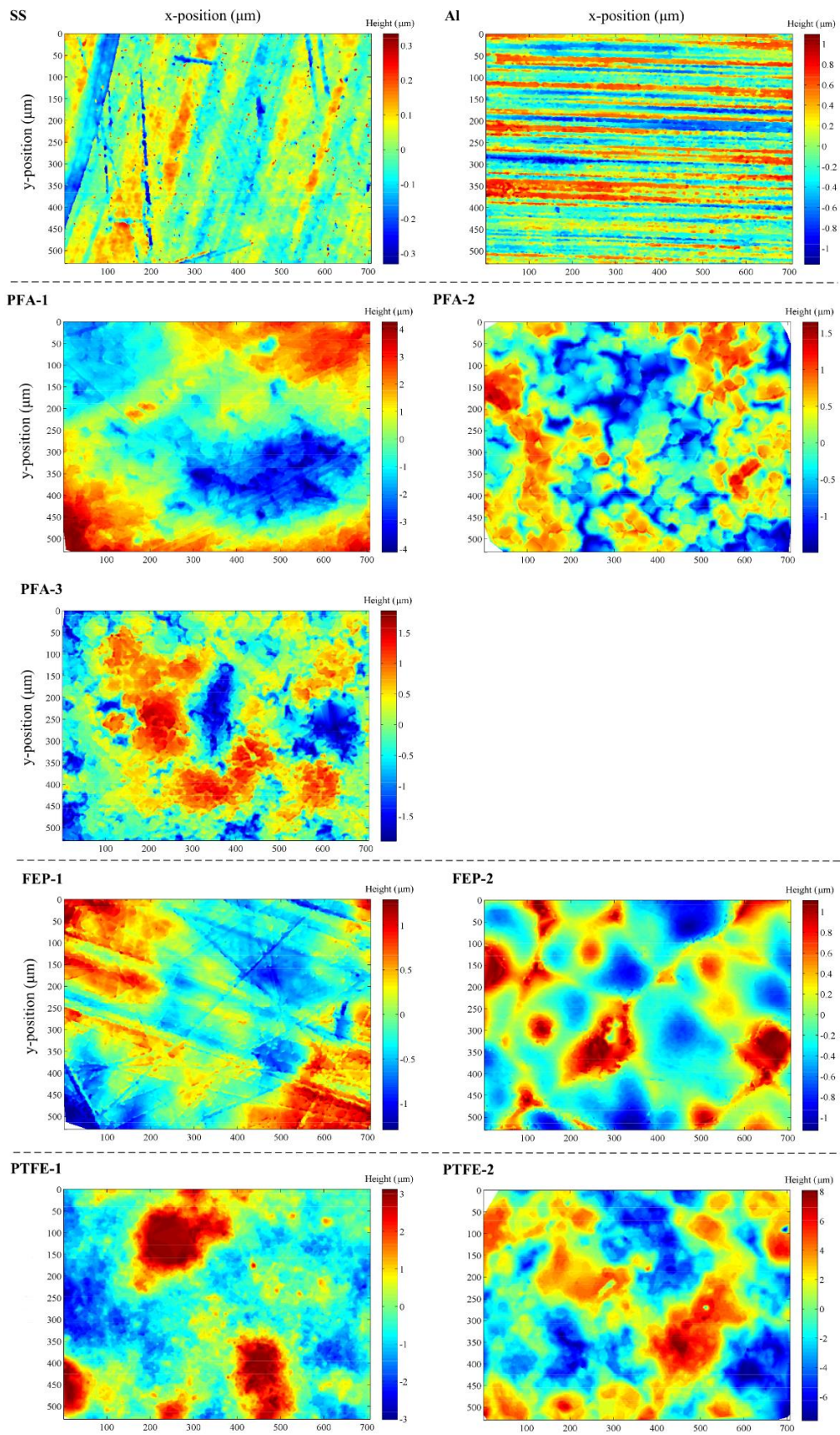


Figure 2: Filtered and interpolated substrate surface topologies. Height scale differs between substrates.

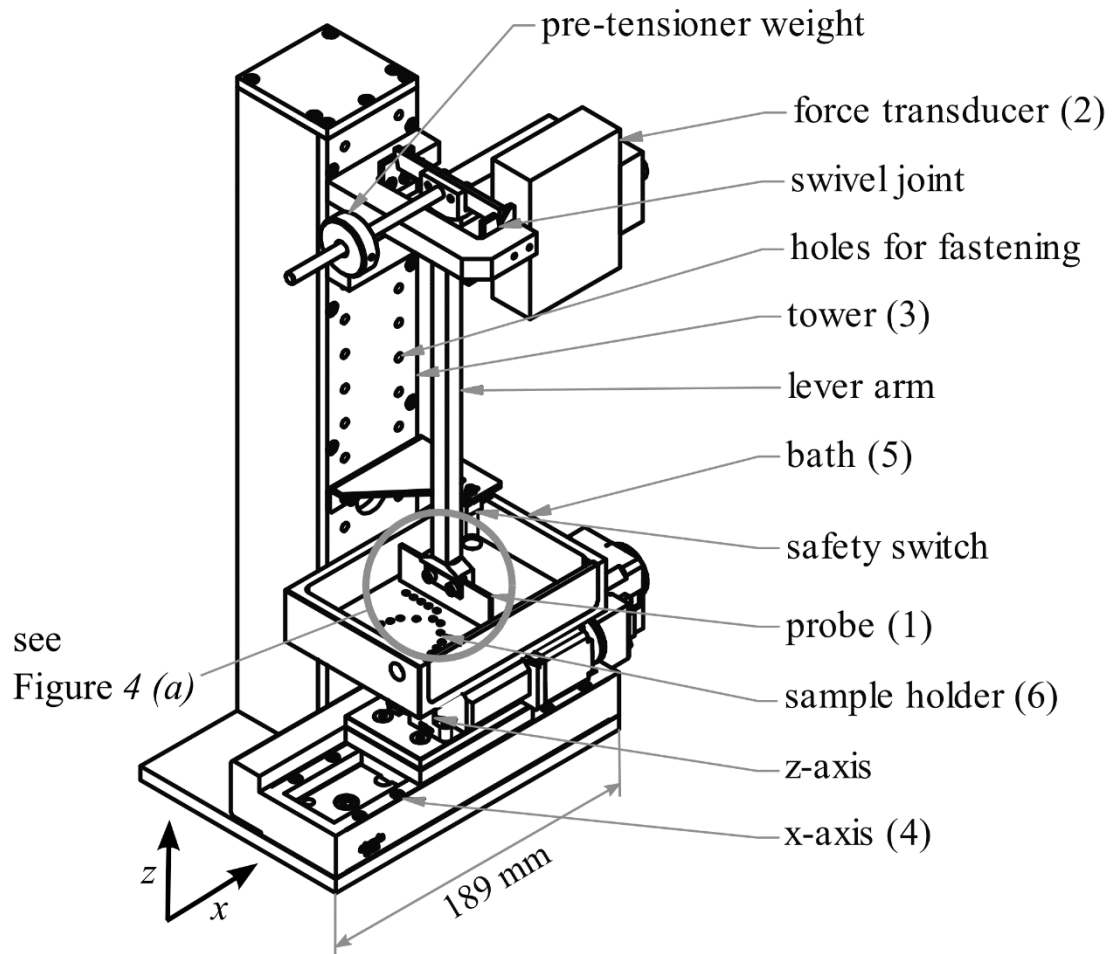
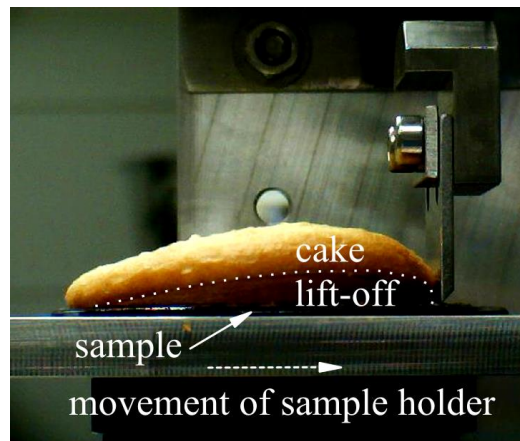


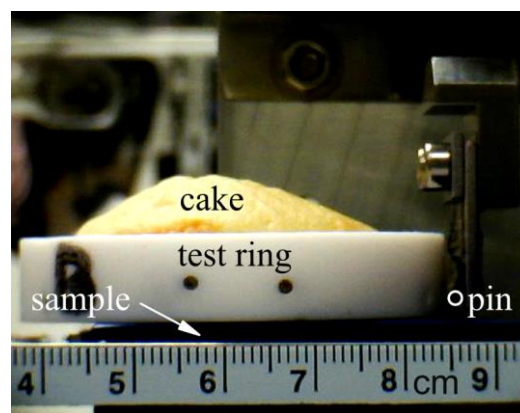
Figure 3: Schematic of the millimanipulation device. Components not shown: axis controllers and force transducer amplifier.

628 (a)



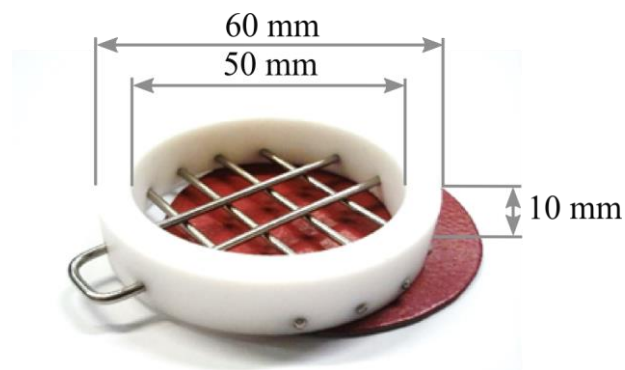
629

630 (b)



631

632 (c)

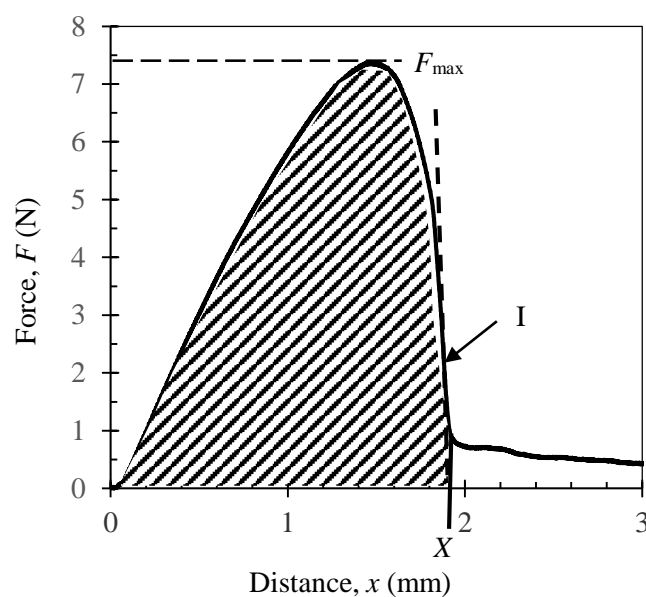


633

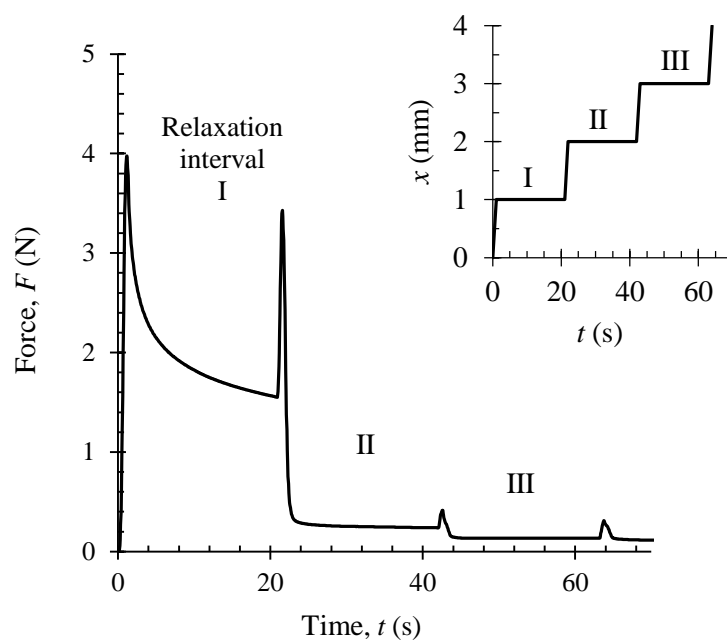
634

635 Figure 4: Millimanipulation of baked cake (a) without and (b) with support ring. Dotted line in (a)
636 shows the cake lifting up, which is prevented in (b) by the support ring detailed in (c) ensuring
637 a defined fracture plane.

638 (a)

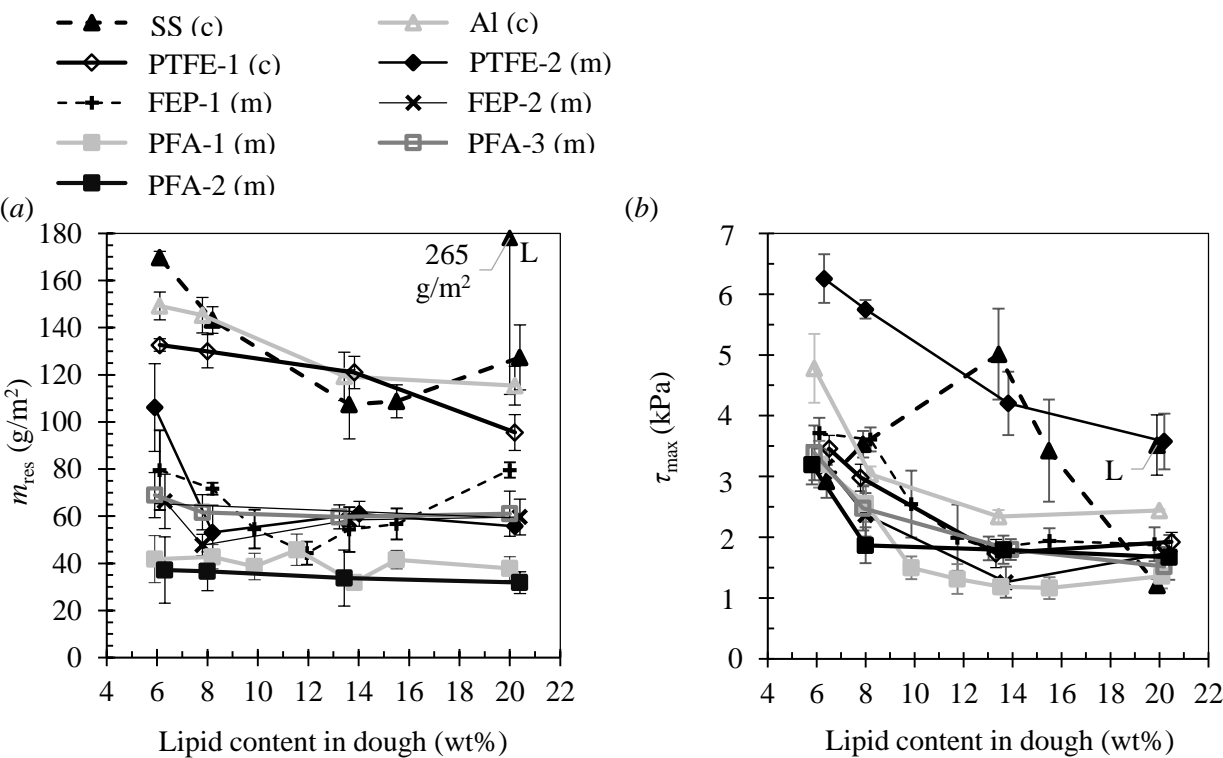


639 (b)
640



641
642 Figure 5: Typical millimanipulation force profiles for shearing of baked cake (PFA-2, 6.11 wt% total
643 lipids). (a) standard test at $v = 1$ mm/s: I marks the point of inflection and X shows the limit of
644 integration to obtain the breakage work with Equation (7). (b) Relaxation test: Inset shows
645 probe motion history, 1 mm/s, 1 mm scrape interval, 20 s stop period.

646



647
648
649

650 Figure 6: Effect of lipid content on (a) residue coverage, and (b) and peak shear force, for nine surfaces.
651 Some markers are offset in lipid content for clarity and connecting lines are reading aids. Datum
652 labelled L indicates anomalous data where lumps of cake were left on SS plates. Legend labels
653 (c) and (m) indicates cohesive and mixed failure, respectively. Error bars show ±1 standard
654 error.
655

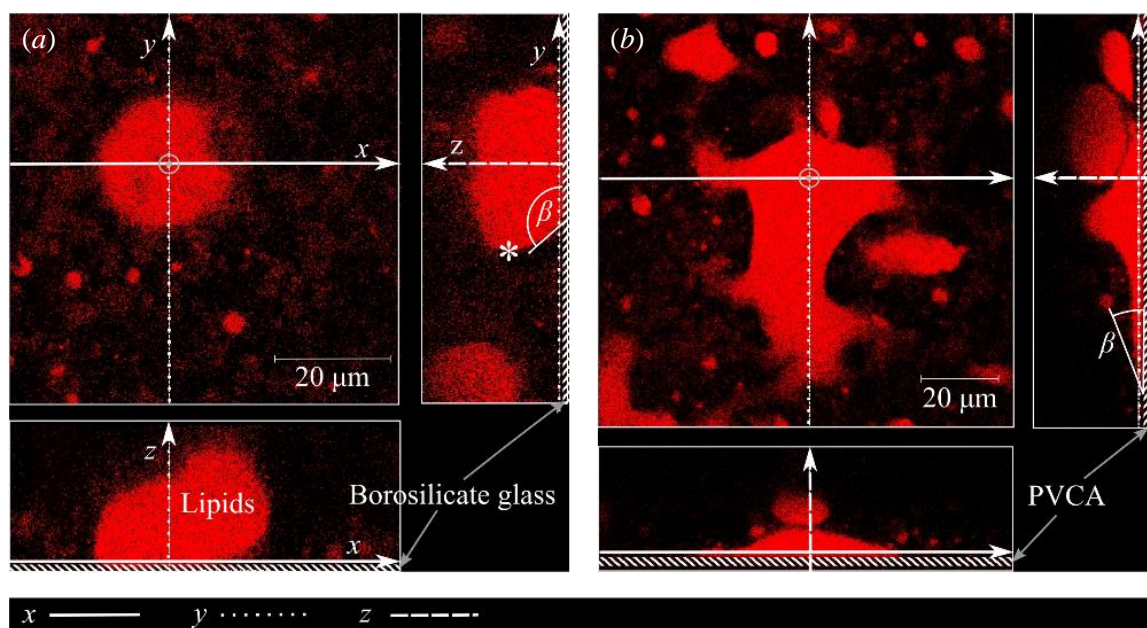


Figure 7: Orthogonal section images obtained by CSLM of cake dough with 8 wt% total lipids on (a) borosilicate glass and (b) PVCA cover slips. Red indicates lipids labelled with Oil Red O.

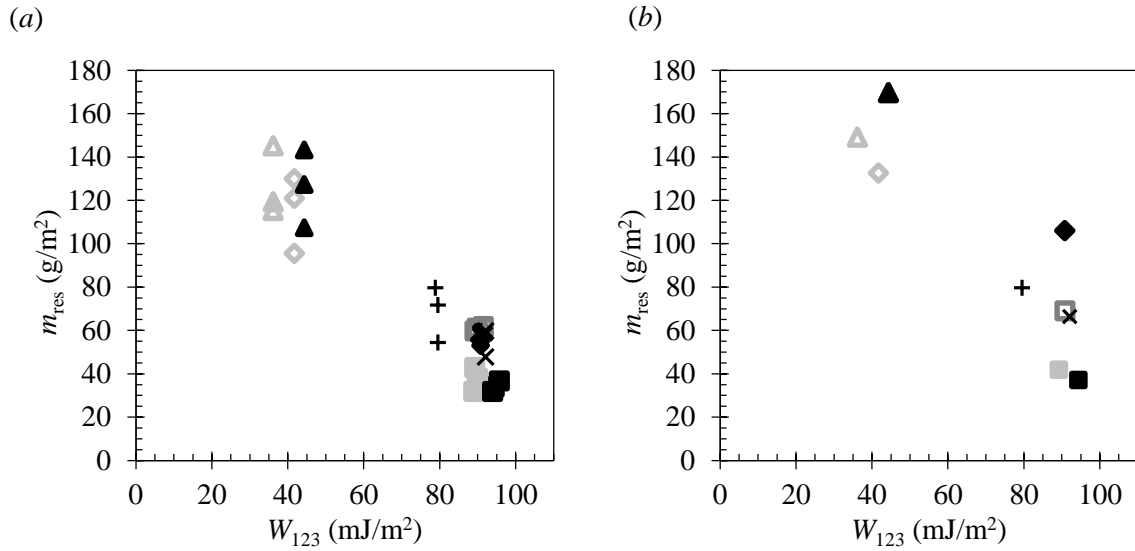
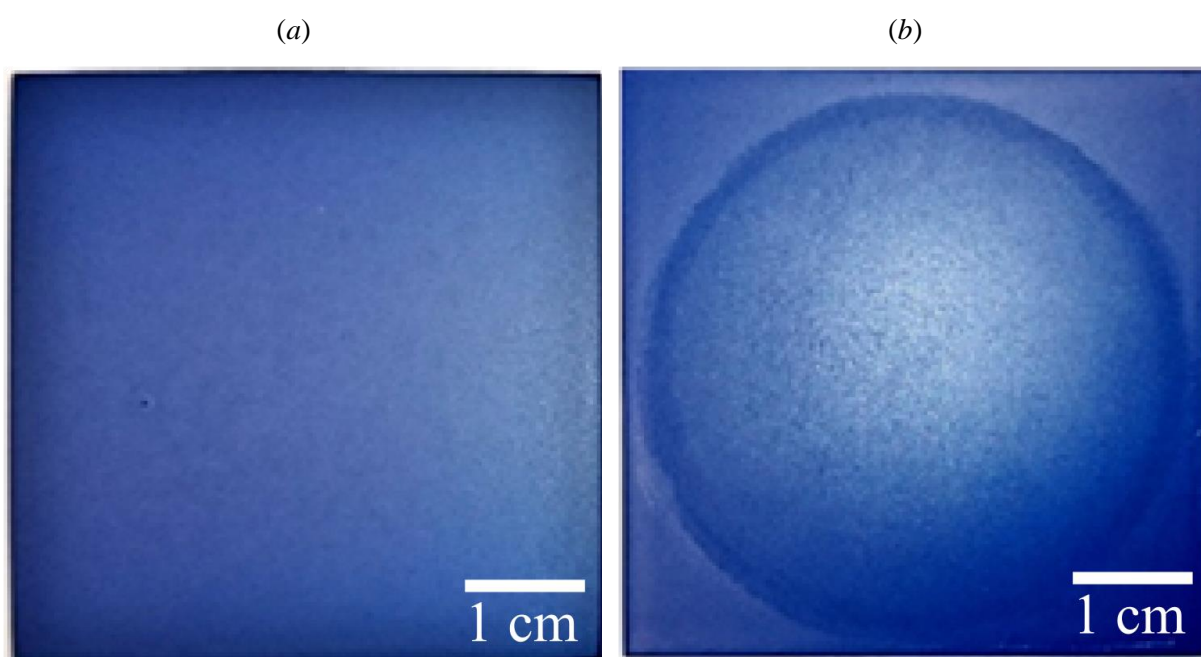


Figure 8: Effect of work of adhesion on residual mass of cake remaining on surface after testing, for (a) cakes containing additional rapeseed oil, total lipid fraction 8, 13.63 or 20.02 wt%, and (b) cakes with no added oil, containing higher melting point lipids from the cake mix (palm fat) and egg powder amounting to 6.11 wt% lipids. W_{123} was calculated using Equation (3) with solid surface energy components from Table 2, oil parameters ($\gamma^d = 33.8$ mJ/m², $\gamma^p = 0$ mJ/m²) and water parameters ($\gamma^d = 21.8$ mJ/m², $\gamma^p = 51.0$ mJ/m²). Symbols given in Table 1.

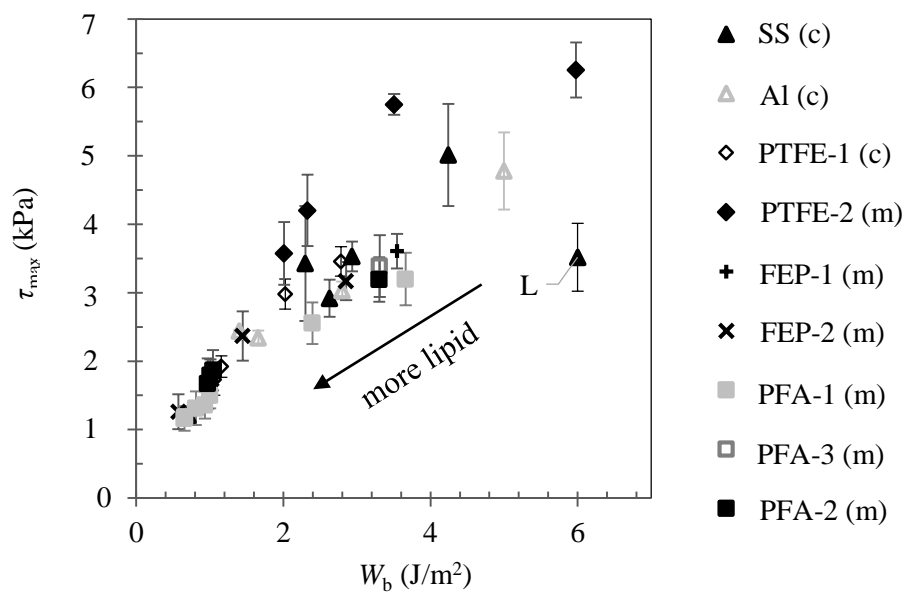
671 Supplementary material 1



672

673 Figure S1: Photographs of PTFE-1 (a) before baking, and (b) cleaned, after first bake.

674

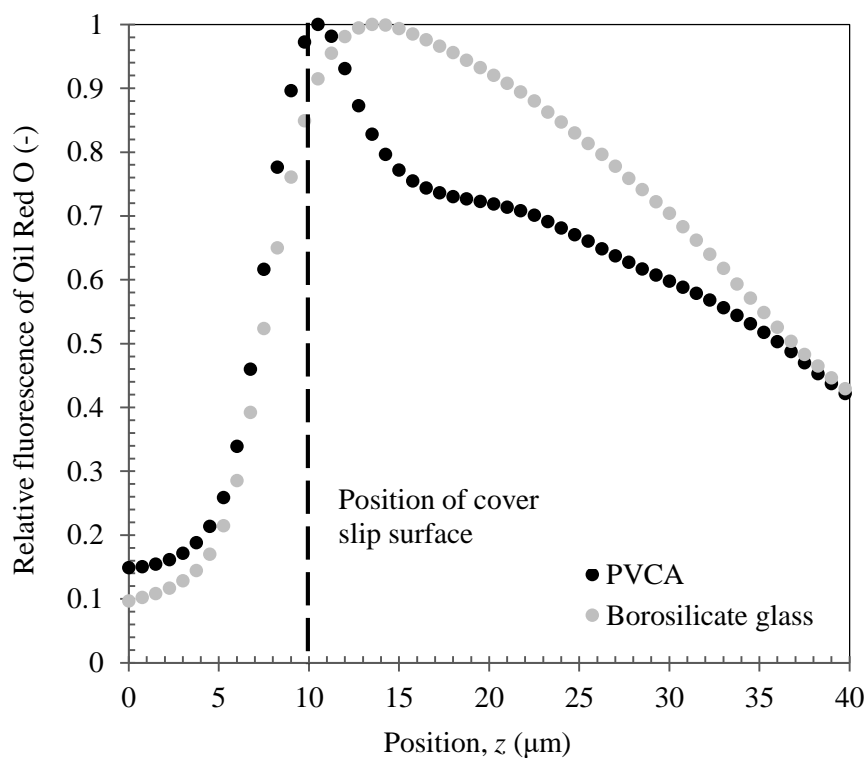


676

677

678 Figure S2: Relationship between peak shear stress and breakage work per unit area for different surfaces
 679 and oil contents. Legend labels (c) and (m) indicate cohesive or mixed failure. Black triangle
 680 labelled with L at 6 J/m^2 indicates anomalous data where lumps of cake were left on SS plates.
 681 Error bars show ± 1 standard error.

683

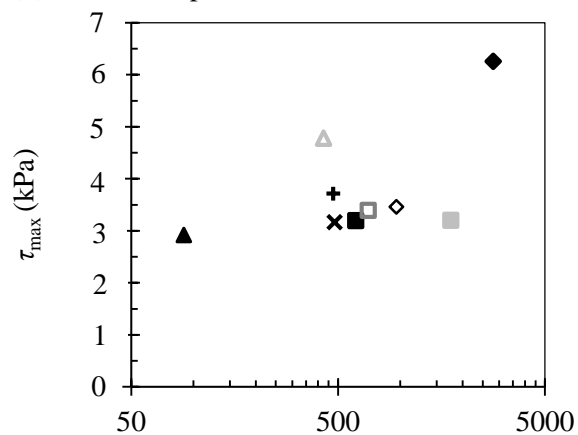


684

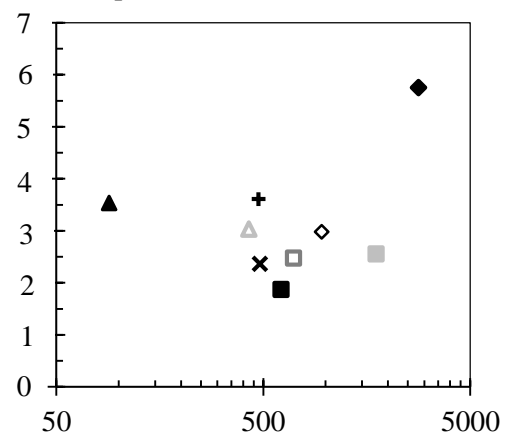
685

686 Figure S3: Distribution of fluorescent material (rapeseed oil dyed with Oil Red O) in the plane paralld
687 to the surface of the cover slips in Figure 11. Scan area 390 x 390 μm . The positions are
688 approximate. The fluorescence intensity was evaluated for each case by calculating the
689 arithmetic mean of intensity values at all locations scanned in the plane a distance z from the
690 surface, then dividing the mean by the highest value obtained for that case.

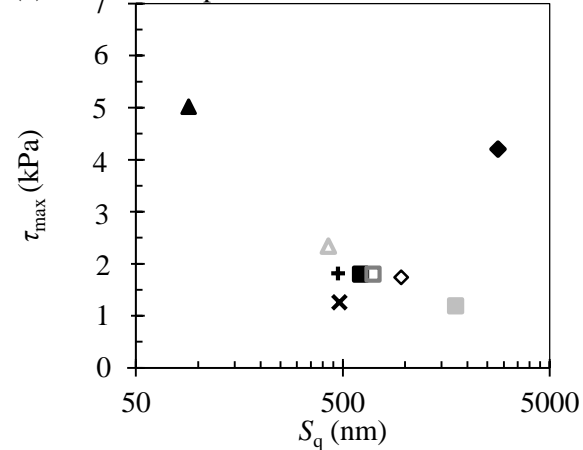
(a) 6.11 wt% lipids



(b) 8 wt% lipids



(c) 13.63 wt% lipids



(d) 20.02 wt% lipids

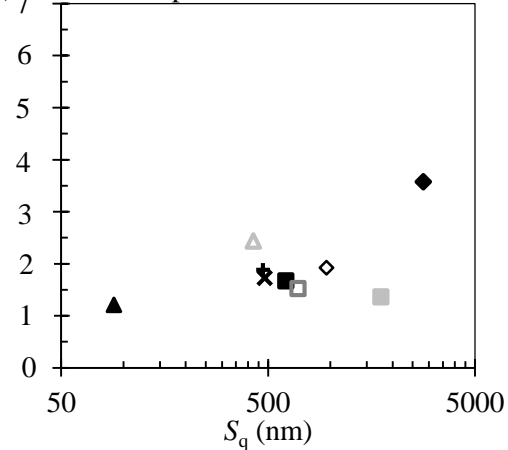


Figure S4: Effect of root mean square surface roughness on peak shear stress for (a) 6.11 wt%, (b) 8 wt%, (c) 13.63 wt% and (d) 20.02 wt% lipids. Symbols given in Table I.